Supporting Information

Regulating the Metal-Support Interaction: Double Jump to Reach the Efficiency Apex of Fe-N_4 Catalyzed Fenton-like Reaction

Jiahao Cui,[†] Lina Li,[†] Siting Shao,[†] Jingyu Gao,[†] Kun Wang,[†] Zhenchun Yang,[†] Shiqi Zeng,[†] Caozheng Diao,[#] Yubao Zhao[†,],and Chun Hu[†]*

[†]Key Laboratory for Water Quality and Conservation of the Pearl River Delta, Ministry of Education & Institute of Environmental Research at Greater Bay, Guangzhou University, 510006 Guangzhou, P. R. China

[#] Singapore Synchrotron Light Source, National University of Singapore,117603 Singapore

***** Email: ybzhao@gzhu.edu.cn

Table of Content

Experimental Procedures

Two-stage architecture engineering of the single-atom Fe catalyst

Synthesis of Fex-CN-TA0.5:

The construction of the polymeric carbon nitride framework was based on the reported method of polymerization of the super-molecular assembly of melamine and cyanuric acid.[1] To synthesize the polymeric carbon nitride supported single-atom Fe catalysts, $FeCl_3 \cdot 6H_2O$ (the amount is denoted by x, and the values are 0, 0.1, 0.25, 0.5, 1.0, 1.5, 2.0 mmol), tannic acid (TA, 0.5 g), cyanuric acid (CA, 5 g), and melamine (MA, 5 g) were dispersed in 400 mL of water, and the mixed under magnetic stirring at room temperature overnight; and the precursor was dried in a vacuum oven at 45 ^oC; the thermal polymerization reaction was conducted in a tube furnace with nitrogen flow at 600 ℃ for 2 h. The as-prepared samples were washed in 0.5 M H_2SO_4 solution for 12 h under room temperature, followed by washing with water until the filtrate being neutral in pH. The polymeric carbon nitride supported single-atom Fe catalysts denoted by Fex-CN-TA0.5 were then collected and dried in a vacuum oven.

Synthesis of Fe1.0-CN-TAy:

The single-atom Fe catalysts were synthesized by varying the amount of TA in the precursor (the amount of TA was denoted by y in gram) via the otherwise same method to the synthesis of *Fe1.0-CN-TA0.5*.

Materials characterizations

The morphology of the catalyst sample was characterized on a JEOL 2100 transmission electron microscope. X-ray diffraction (XRD) patterns of the catalysts were obtained on a Rigaku D/MAX 2500 diffractometer with Cu radiation (Cu Kα = 0.15406 nm). X-ray photoelectron spectroscopy (XPS) analysis was conducted on an ESCA laboratory 220i-XL spectrometer; all the binding energy were calibrated to C 1s peak at 284.8 eV. The concentration of Fe was quantified by inductively coupled plasma - optical emission spectrometer (ICP-OES) (PerkinElmer, AVIO 200).

Evaluation of the catalytic performance

In a typical experiment of catalytic PMS activation for the pollutant degradation, 8 mg catalyst was dispersed in 50 mL BPA solution by ultrasonication for 10 min, followed by mixing by magnetic stirrer in dark for 15 min to reach the adsorption-desorption equilibrium. It has been experimentally confirmed that 15 min was more than enough for reaching the equilibrium. The suspension was sampled for initial BPA concentration analysis. The catalytic reaction was initiated by dropping the PMS stock solution (1 M), and the initial PMS concentration was 1 mM, unless otherwise stated. The suspension was sample at specific intervals, the catalyst was removed by syringe filter, and the filtrated was mixed with methanol for pollutants concentration analysis with HPLC. If not specified, the initial pH of the solution was around 6.5. HPLC analysis were performed on Shimazu SIL-20A HPLC with Shim-pack GIST C18 column (4.6×250 mm, 5 μm). Mobile phase and detection wavelength setting for the pollutants: bis phenol A (BPA), methanol/water (70/30) and λ = 225 nm; sulfamethoxazole, methanol/water (55/45) and λ = 266 nm; 4-chloro-phenol, phosphate acid solution (0.08%)/acetonitrile (50/50) and λ = 221 nm; methyl phenyl sulfoxide (MPSO), phosphate acid solution (0.08%)/acetonitrile (70/30) and λ = 215 nm.

Electron spin resonance (ESR) experiments

For detecting the free radicals in the bulk solution, 5,5-Dimethyl-2-pyrrolidone-N-oxyl (DMPO) was employed as the spin-trapping agent. In a typical analysis, 0.22 mL DMPO was added into 11 mL PMS solution with concentration of 1.0 mM in a glass vial with volume of 15 mL under magnetic stirring. One millilitre solution was then sampled and measured by ESR as the blank experiment. 1.5 mg catalyst was then added in the glass vial to initiate the reaction. After 20 s of reaction time, the suspension was sampled, filtered, and sealed in a capillary tube for ESR data collection. For detecting the singlet oxygen ($^1O_2$) in the reaction system, 2,2,6,6-tetramethylpiperidine (TEMP) was employed as the spin-trapping agent. In a typical experiment, 11 mL solution with 1 mM PMS, 10 mM TEMP, and 20 ppm BPA was magnetically stirred in a glass via with capacity of 15 mL. 7.5 mg catalyst was added in the glass vial to start the reaction. At specified interval, 1 mL suspension was sampled, filtered, and sealed in a capillary tube for ESR data collection.

Theoretical simulations

All the first-principles spin-polarized calculations were performed by using the Vienna ab initio Simulation Program (VASP).[2-3] The generalized gradient approximation (GGA) in the Perdew-

Burke-Ernzerhof (PBE) form and a cutoff energy of 500 eV for planewave basis set were adopted.[4] A 5 × 5 × 1 Monkhorst-Pack k grid was used for sampling the Brillouin zones at structure calculation.[5] The ion-electron interactions were described by the projector augmented wave (PAW) method.[6] The convergence criteria of structure optimization were choose as the maximum force on each atom less than 0.02 eV/Å with an energy change less than 1×10^{-5} eV. To calculate the kinetic energy barrier of chemical reactions, the climbing image nudged elastic band (CI-NEB) method was used to search for the transition states.[7]

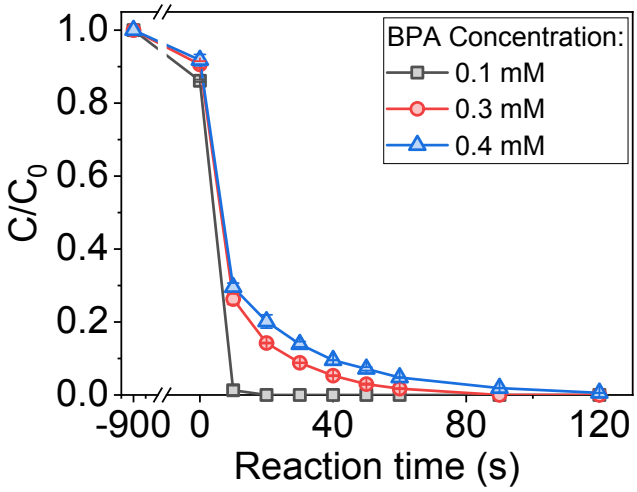

Figure S1. Degradation of BPA at a series of concentrations on Fe1.0-CN-TA2.0.

Reaction conditions: [catalyst] = 0.16 g L−1; [PMS] = 1.0 mM; initial pH = 6.5.

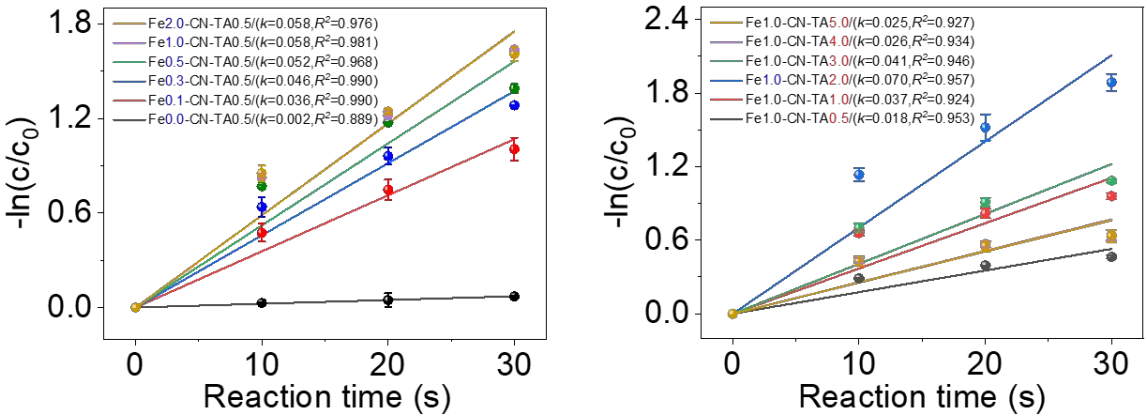

Figure S2. Pseudo first-order reaction kinetics fitting of the reactions. Degradation of BPA at a series of concentrations on Fe1.0-CN-TA2.0.

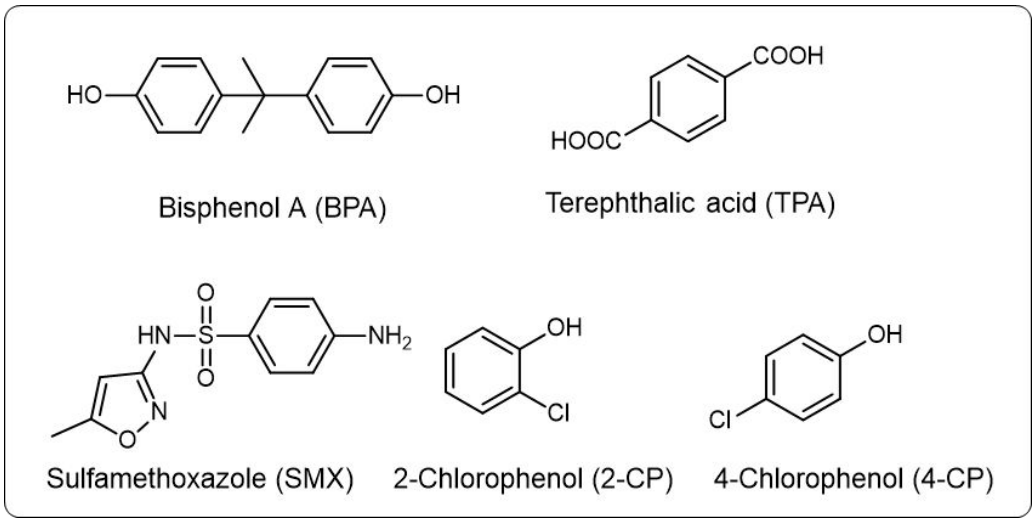

Figure S3. Molecular structure of the selected pollutants.

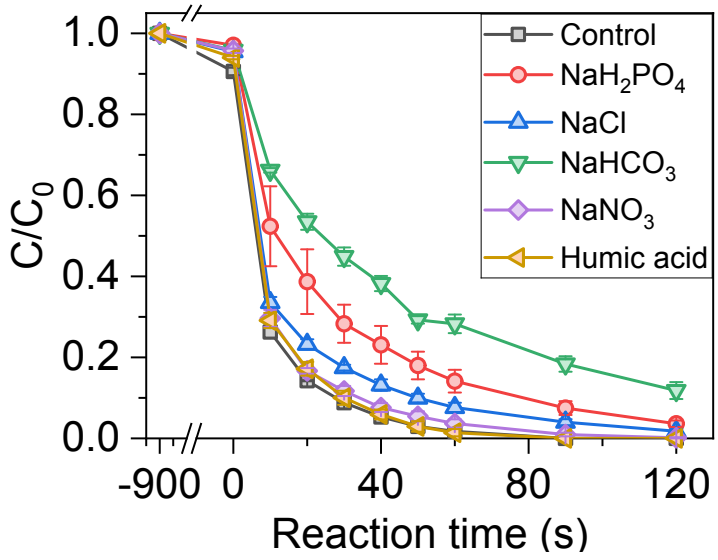

Figure S4. The impact of the mineral ions and humic acid on BPA degradation performance on Fe1.0-CN-TA2.0.

Reaction conditions: [catalyst] = 0.16 g L^{-1}, [BPA] = 0.3 mM, [anion] = 5 mM, [humic acid] = 5 mg L^{-1}, [PMS] = 1.0 mM.

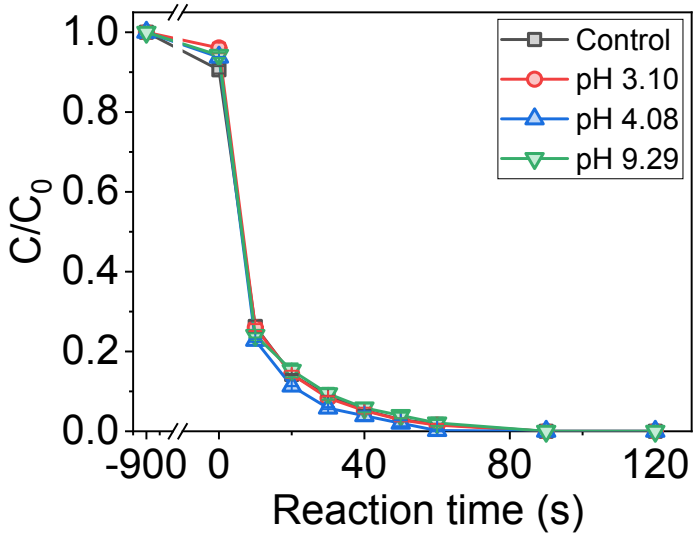

Figure S5. The impact of the initial pH on BPA degradation performance on Fe1.0-CN-TA2.0.

Reaction conditions: [catalyst] = 0.16 g L^{-1}, [BPA] = 0.3 mM, [PMS] = 1.0 mM, initial pH = 6.5.

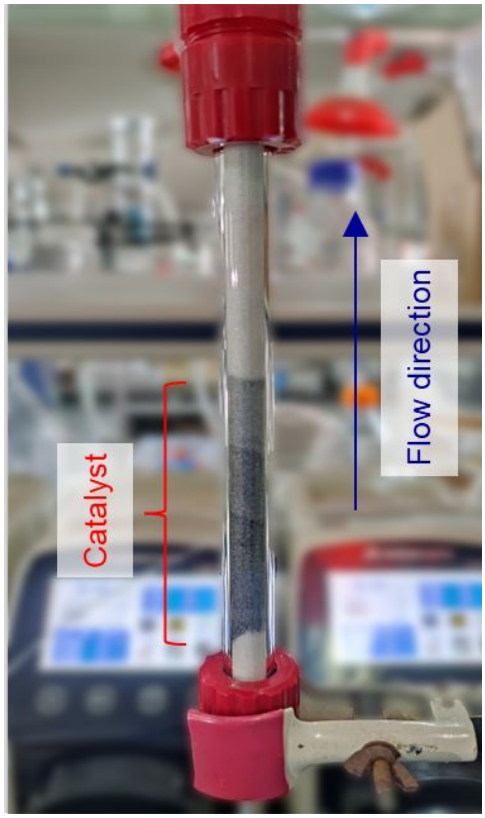

Figure S6. Photograph of the fixed-bed flow reactor setup.

Reaction conditions: catalyst loading, 20 mg; [PMS] = 0.5 mM; [BPA] = 0.1 mM; flow rate, 12.0 mL h^{-1}.

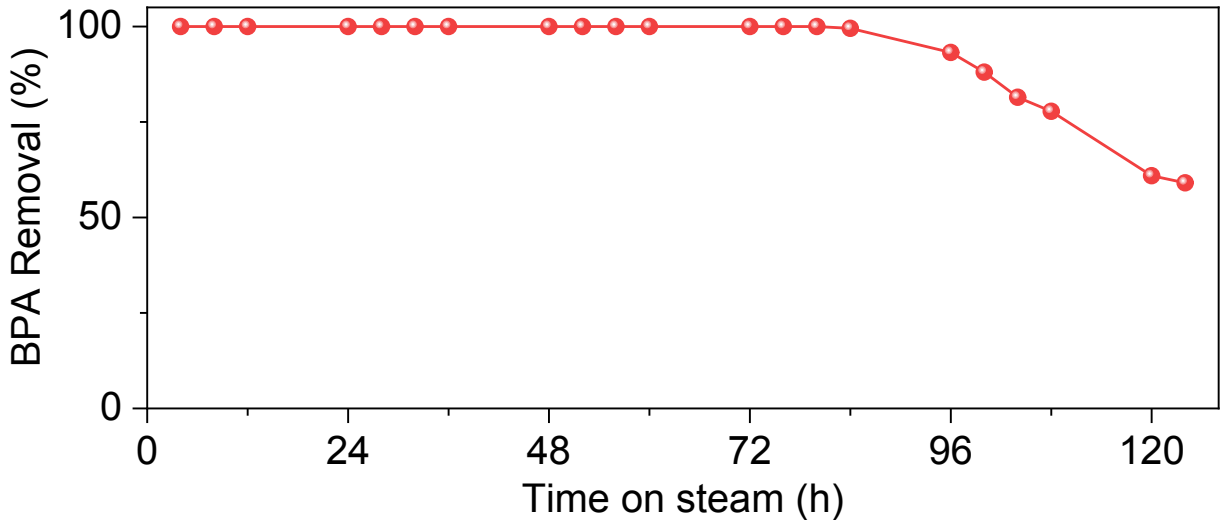

Figure S7. The performance of Fe1.0-CN-TA2.0 in a fixed-bed flow reactor for catalytic BPA removal in Pear River water.

Location for water sampling: (23°02'07.4"N, 113°22'07.2"E). Date: October 06, 2022.

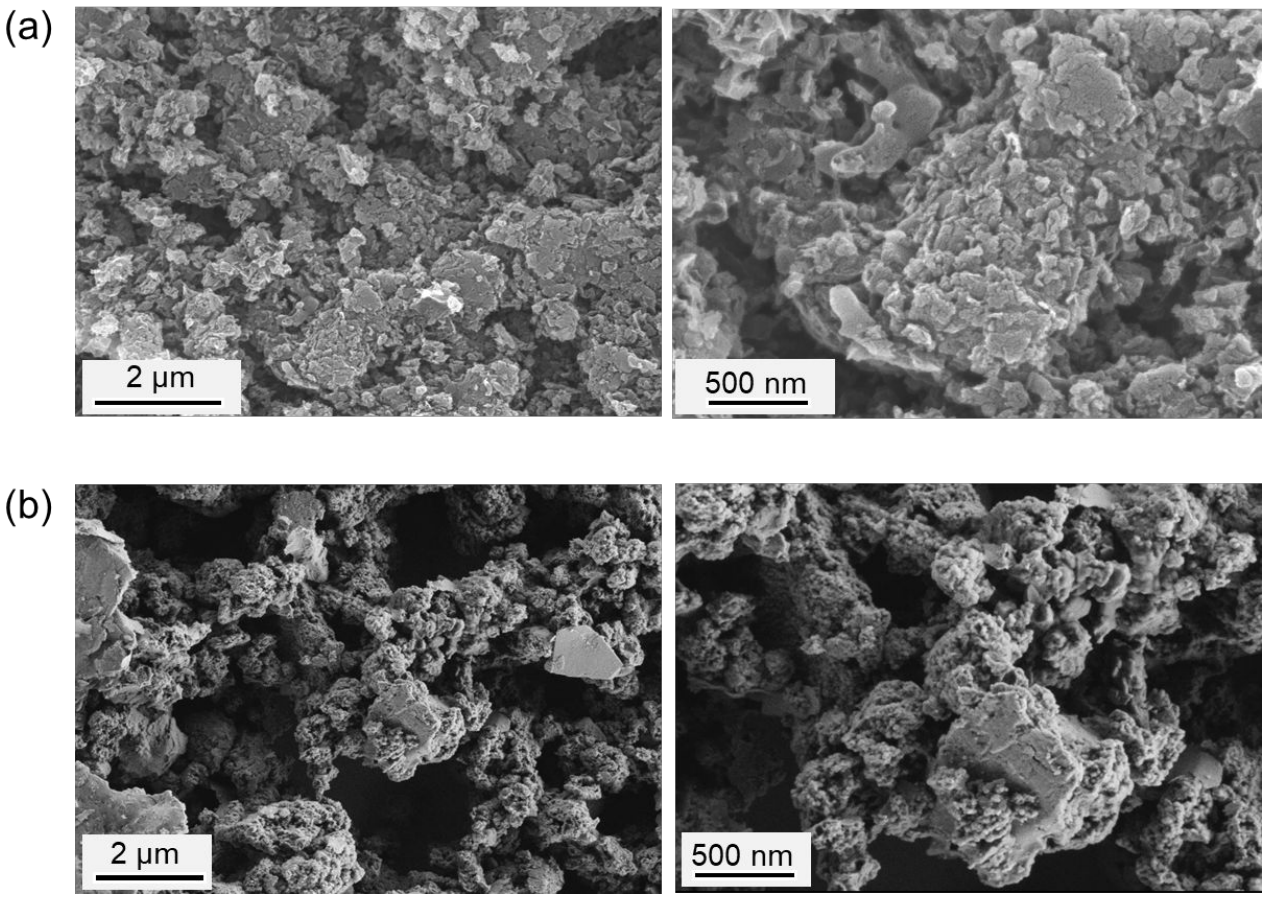

Figure S8. Scanning electronic microscopy images of Fe1.0-CA-TA2.0 before (a) and after (b) reaction.

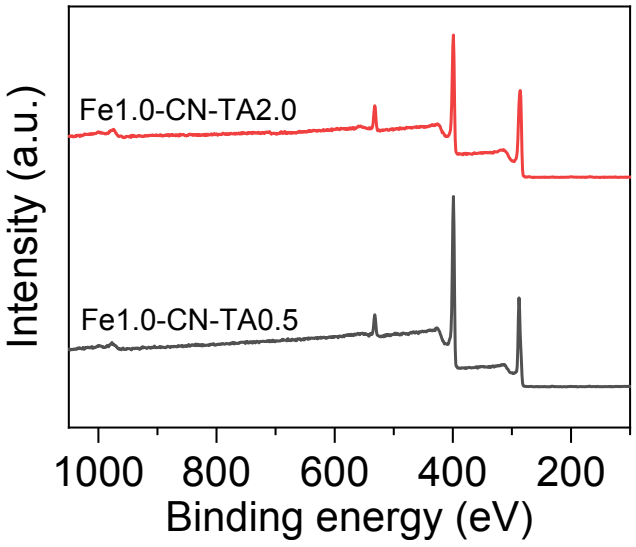

Figure S9. X-ray photoelectron spectroscopy (XPS) survey scan of the catalysts.

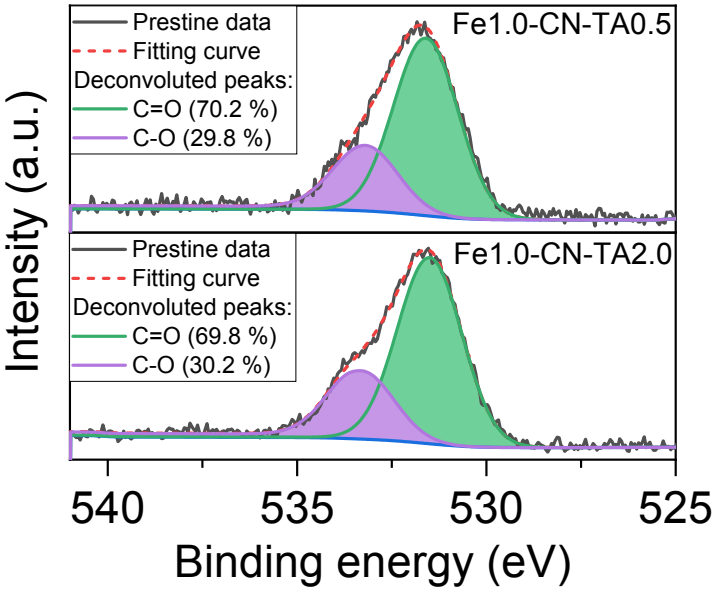

Figure S10. X-ray photoelectron spectra of O 1s signal.

C=O: 531.6 eV: oxygen doubly bound to carbon (i.e., C=O) in quinones, ketones, and aldehydes; C-O: 533.2 eV oxygen singly bound to carbon (i.e., C-O) in ethers and phenols. [8-9]

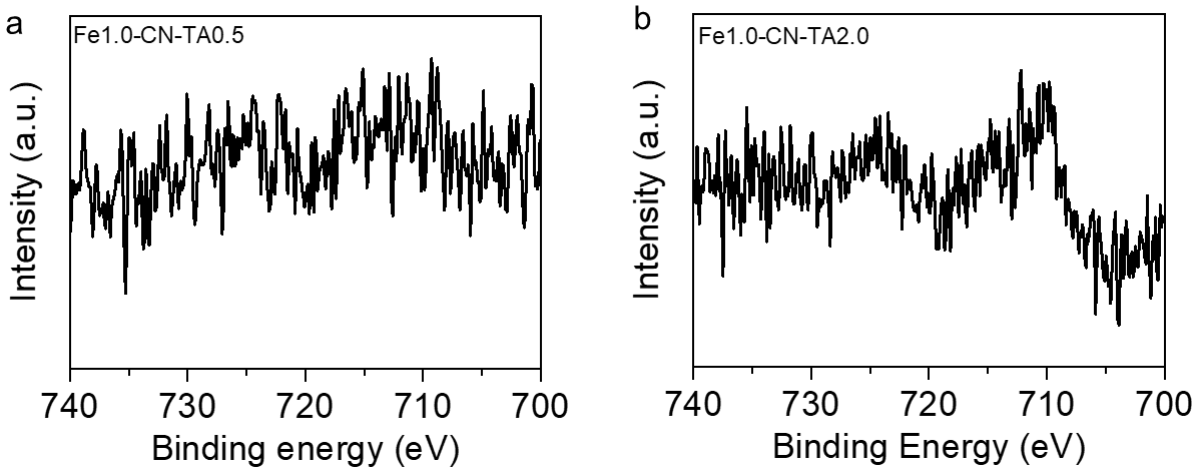

Figure S11. X-ray photoelectron spectra of Fe 2p signals.

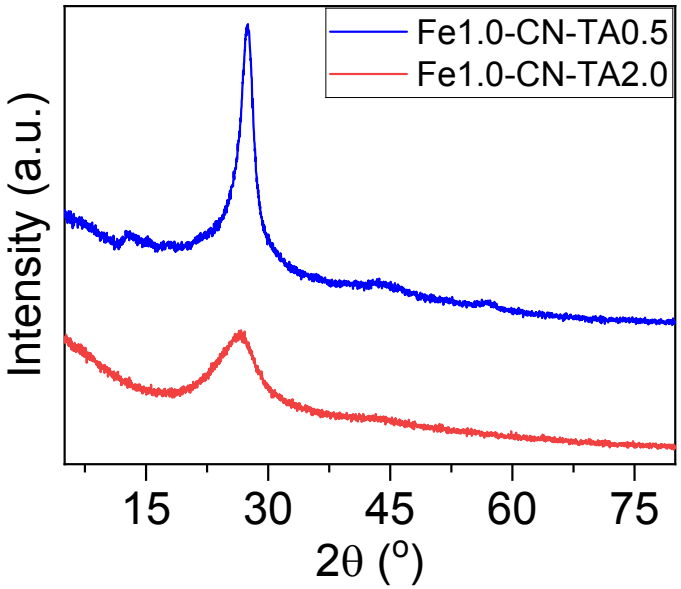

Figure S12. X-ray diffraction (XRD) profiles of the catalysts.

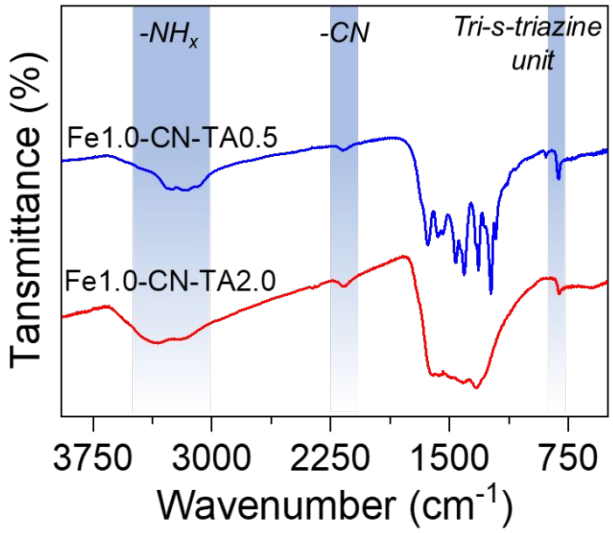

Figure S13. Fourier transform infrared (FT-IR) spectra of the catalysts.

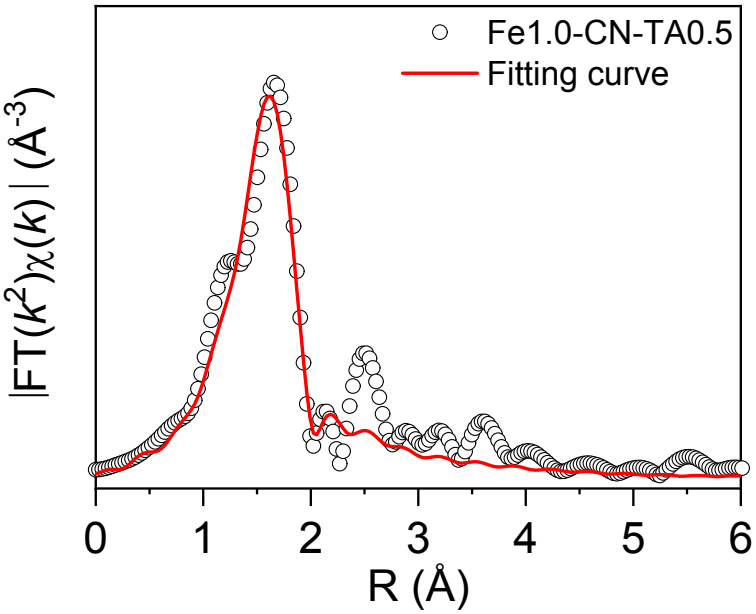

Figure S14. Fe K-edge Fourier transform EXAFS spectrum of Fe1.0-NC-TA0.5 and the fitting curve.

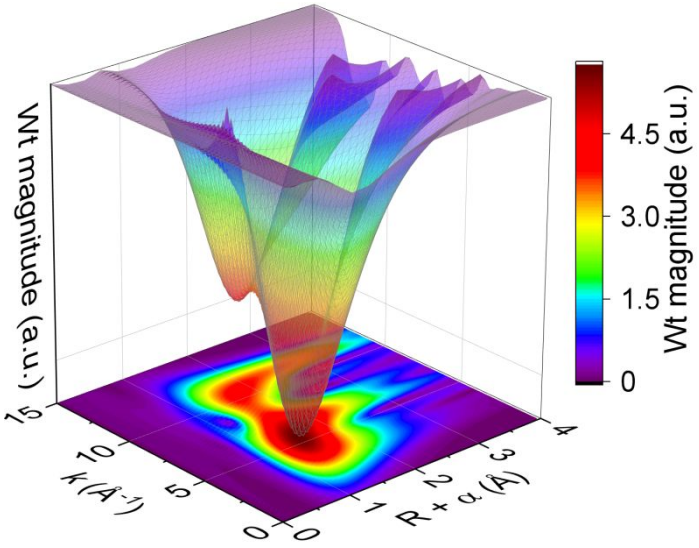

Figure S15. Wavelet transforms of the k^2-weighted EXAFS of Fe1.0-CN-TA0.5.

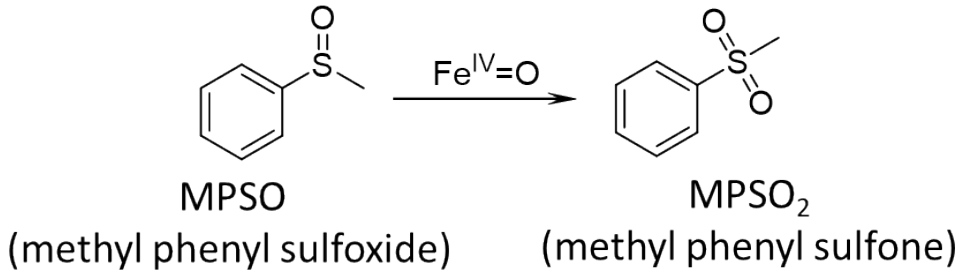

Figure S16. The selective conversion of MPSO to $MPSO_2$ by high valent Fe^{IV}=O.

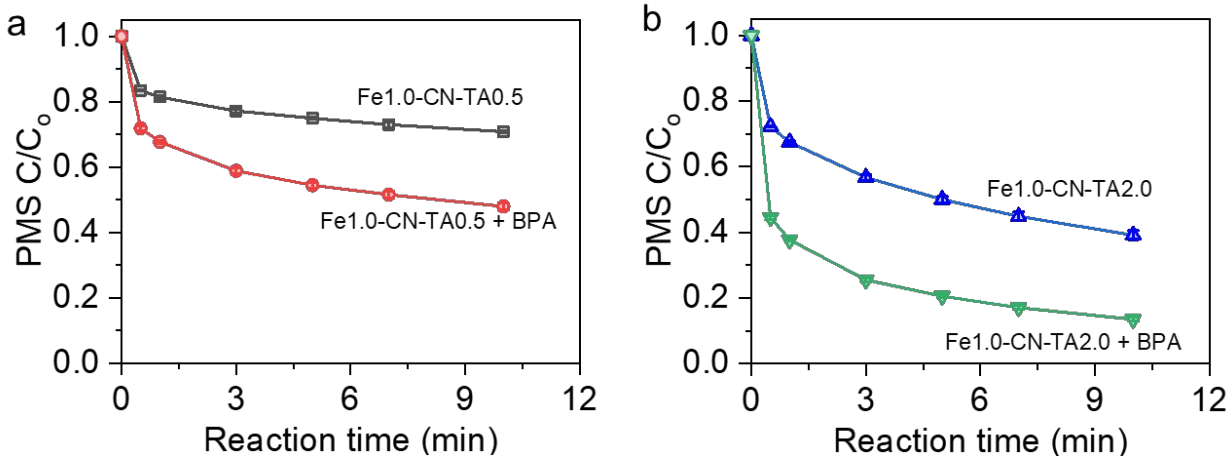

Figure S17. The impact of BPA on the PMS consumption on the single-atom Fe catalysts.

Reaction conditions: [catalyst] = 0.16 g L^{-1}; [PMS] = 1.0 mM; [BPA] = 0.3 mM, if any. Initial pH, 6.5.

Table S1. Summary of the recently reported single-atom catalysis for PMS activation.

Catalyst (Loading / g L^{-1})	Pyrolysis temperature (^oC)	[BPA] (μM)	[PMS] (mM)	Removal efficiency	References
Fe1.0-CN-TA2.0 (0.16)	600	300	1.0	100%(1.5 min)	This Work
CoSA/NHCS (0.1)	600	87.61	0.33	100%(2 min)	10
Co−N_4−C (0.1)	950	87.61	0.5	100%(10 min)	11
SA-CoCN-1.0 (0.3)	520	43.80	0.5	100%(30 min)	12
ZIF-8@67-C (0.1)	950	87.61	0.33	91.62%(0.25 min)	13
FeCo-NC-2 (0.1)	650	87.61	0.65	100%(4 min)	14
Fe_{SA}-N-C (0.15)	900	87.61	1.30	100%(30 min)	15
Mn-ISAs@CN (0.2)	900	87.61	0.65	100%(4 min)	16
Co-Sas (0.2)	800	87.61	1.30	81.6%(12 min)	17
Fe_{SA}-N/C-20 (0.15)	900	87.61	1.30	100%(20 min)	18
p-$CoSi_1N_3$@D (0.02)	900	87.61	0.4	99%(5 min)	19
Co-TPML (0.2)	800	50	2	100%(5 min)	20
SA Co-N/C (0.05)	1000	43.8	0.5	100%(15 min)	21
$CoCN_{-0.4z1m}$ (0.2)	600	87.61	0.65	100%(20 min)	22
CoNPC-7.78 (0.05)	1000	87.61	1.6	100%(5 min)	23
3SACu@NBC (0.1)	900	87.61	1.30	100%(30 min)	24
Co-N-C-900 (0.5)	900	0.35	0.976	100%(3 min)	25
Fe_{SA}-N-CNT (0.02)	700	50	0.4	100%(1 min)	26
SA-Fe-NC (0.05)	800	100	2	100%(3 min)	27
FeSA-N/O-C (0.1)	600	65.71	0.3	100%(45 min)	28
p-MnNC@Mt-900 (0.1)	900	43.8	0.6	100%(5 min)	29
Co-N_2 (0.2)	1000	50	2	100%(5 min)	30
SA-Fe/CN (0.02)	900	20	0.1	100%(5 min)	31
SA-Cu-NC (0.04)	800	50	1.0	95%(60 min)	32
Cu-SA (0.1)	800	100	0.5	60%(5 min)	33

Table S2. Weight percentage of Fe in the single-atom Fe catalysts.

Entry	Catalyst	Fe loadings (wt. %)
1	Fe0.1-CN-TA0.5	0.13
2	Fe0.3-CN-TA0.5	0.37
3	Fe0.5-CN-TA0.5	0.73
4	Fe1.0-CN-TA0.5	1.19
5	Fe2.0-CN-TA0.5	1.09
6	Fe1.0-CN-TA1.0	2.27
7	Fe1.0-CN-TA2.0	2.43
8	Fe1.0-CN-TA3.0	2.22
9	Fe1.0-CN-TA4.0	1.72
10	Fe1.0-CN-TA5.0	1.79

Table S3. Percentage of the deconvoluted peaks in the XPS C 1s signal.

Entry	Component	Percentage (%)	
		Fe1.0-CN-TA0.5	Fe1.0-CN-TA2.0
1	C= C	21.1	39.6
2	C−C	12.1	25.0
3	N=C−N	57.4	24.2
4	C=O, C=N	9.4	11.2

Table S4. Percentage of the deconvoluted peaks in the XPS N1s signal.

Entry	Component	Percentage (%)	
		Fe1.0-CN-TA0.5	Fe1.0-CN-TA2.0
1	C=N−C	64.0	53.4
2	N−(C3)	18.1	23.4
3	C−N−H	17.9	23.2

Table S5. Percentage of the C, N, and O determined by XPS.

Entry	items	Percentage (%)	
		Fe1.0-CN-TA0.5	Fe1.0-CN-TA2.0
1	C	46.6	55.9
2	N	49.3	38.8
3	O	4.0	5.1
4	C/N	0.95	1.44

Table S6. EXAFS fitting parameters for Fe1.0-CN-TA2.0.

Shell	CN [a]	R (Å) [b]	σ^2 (Å^2) [c]	ΔE_0 (eV) [d]	R factor [e]
Fe−N	3.56	2.07± 0.02	0.0101± 0.0020	1.773	0.0117

[a] CN: Coordination number. [b] R: Bond distance. [c] σ^2: Debye-Waller factor. [d] ΔE_0: the inner potential correction. [e] R factor: the goodness of fitting.

Table S7. EXAFS fitting parameters for Fe1.0-CN-TA0.5.

Shell	CN [a]	R(Å) [b]	σ^2 (Å^2) [c]	ΔE_0 (eV) [d]	R factor [e]
Fe−N	3.47	2.08 ± 0.02	0.0106± 0.0025	2.715	0.0131

[a] CN: Coordination number. [b] R: Bond distance. [c] σ^2: Debye-Waller factor. [d] ΔE_0: the inner potential correction. [e] R factor: the goodness of fitting.

References:

1. Shalom, M.; Inal, S.; Fettkenhauer, C.; Neher, D.; Antonietti, M., Improving carbon nitride photocatalysis by supramolecular preorganization of monomers. *J. Am. Chem. Soc.* 2013, *135* (19), 7118-7121.
2. Kresse, G.; Furthmüller, J., Efficiency of ab-initio total energy calculations for metals and semiconductors using a plane-wave basis set. *Comput. Mater. Sci.* 1996, *6* (1), 15-50.
3. Kresse, G.; Furthmüller, J., Efficient iterative schemes for ab initio total-energy calculations using a plane-wave basis set. *Phys. Rev. B* 1996, *54* (16), 11169-11186.
4. Perdew, J. P.; Burke, K.; Ernzerhof, M., Generalized gradient approximation made simple. *Phys. Rev. Lett.* 1996, *77* (18), 3865-3868.
5. Monkhorst, H. J.; Pack, J. D., Special points for Brillouin-zone integrations. *Phys. Rev. B* 1976, *13* (12), 5188-5192.
6. Blöchl, P. E., Projector augmented-wave method. *Phys. Rev. B* 1994, *50* (24), 17953-17979.
7. Henkelman, G.; Uberuaga, B. P.; Jónsson, H., A climbing image nudged elastic band method for finding saddle points and minimum energy paths. *J. Chem. Phys.* 2000, *113* (22), 9901-9904.
8. Kundu, S.; Wang, Y.; Xia, W.; Muhler, M., Thermal stability and reducibility of oxygen-containing functional groups on multiwalled carbon nanotube surfaces: A quantitative high-resolution XPS and TPD/TPR study. *J. Phys. Chem. C* 2008, *112* (43), 16869-16878.
9. Lu, Z.; Chen, G.; Siahrostami, S.; Chen, Z.; Liu, K.; Xie, J.; Liao, L.; Wu, T.; Lin, D.; Liu, Y.; Jaramillo, T. F.; Nørskov, J. K.; Cui, Y., High-efficiency oxygen reduction to hydrogen peroxide catalysed by oxidized carbon materials. *Nat. Catal.* 2018, *1* (2), 156-162.

10. Xu, Z.; Zhang, Y.; Wang, F.; Li, Z.; Gu, W.; Zhang, Y.; Xie, H., Co single-atom confined in N-doped hollow carbon sphere with superb stability for rapid degradation of organic pollutants. *Chem. Eng. J.* 2023, *452*, 139229.
11. Yang, M.; Hou, Z.; Zhang, X.; Gao, B.; Li, Y.; Shang, Y.; Yue, Q.; Duan, X.; Xu, X., Unveiling the origins of selective oxidation in single-atom catalysis via Co–N_4–C intensified radical and nonradical pathways. *Environ. Sci. Technol.* 2022, *56* (16), 11635-11645.
12. Wang, Q.; Liu, C.; Zhou, D.; Chen, X.; Zhang, M.; Lin, K., Degradation of bisphenol a using peroxymonosulfate activated by single-atomic cobalt catalysts: Different reactive species at acidic and alkaline pH. *Chem. Eng. J.* 2022, *439*, 135002.
13. Zhu, C.; Nie, Y.; Zhao, S.; Fan, Z.; Liu, F.; Li, A., Constructing surface micro-electric fields on hollow single-atom cobalt catalyst for ultrafast and anti-interference advanced oxidation. *Appl. Catal. B* 2022, *305*, 121057.
14. Li, X.; Huang, X.; Xi, S.; Miao, S.; Ding, J.; Cai, W.; Liu, S.; Yang, X.; Yang, H.; Gao, J.; Wang, J.; Huang, Y.; Zhang, T.; Liu, B., Single cobalt atoms anchored on porous N-doped graphene with dual reaction sites for efficient fenton-like catalysis. *J. Am. Chem. Soc.* 2018, *140* (39), 12469-12475.
15. Li, Y.; Yang, T.; Qiu, S.; Lin, W.; Yan, J.; Fan, S.; Zhou, Q., Uniform N-coordinated single-atomic iron sites dispersed in porous carbon framework to activate PMS for efficient BPA degradation via high-valent iron-oxo species. *Chem. Eng. J.* 2020, *389*, 124382.
16. Yang, J.; Zeng, D.; Zhang, Q.; Cui, R.; Hassan, M.; Dong, L.; Li, J.; He, Y., Single Mn atom anchored on N-doped porous carbon as highly efficient Fenton-like catalyst for the degradation of organic contaminants. *Appl. Catal. B* 2020, *279*, 119363.
17. Gao, Y.; Yang, C.; Zhou, M.; He, C.; Cao, S.; Long, Y.; Li, S.; Lin, Y.; Zhu, P.; Cheng, C., Transition metal and metal–Nx codoped MOF-derived Fenton-like catalysts: A comparative study on single atoms and nanoparticles. *Small* 2020, *16* (50), 2005060.
18. Yang, T.; Fan, S.; Li, Y.; Zhou, Q., Fe-N/C single-atom catalysts with high density of Fe-Nx sites toward peroxymonosulfate activation for high-efficient oxidation of bisphenol A: Electron-transfer mechanism. *Chem. Eng. J.* 2021, *419*, 129590.
19. Dong, X.; Chen, Z.; Tang, A.; Dionysiou, D. D.; Yang, H., Mineral modulated single atom catalyst for effective water treatment. *Adv. Funct. Mater.* 2022, *32* (16), 2111565.
20. Chu, C.; Yang, J.; Zhou, X.; Huang, D.; Qi, H.; Weon, S.; Li, J.; Elimelech, M.; Wang, A.; Kim, J.-H., Cobalt single atoms on tetrapyridomacrocyclic support for efficient peroxymonosulfate activation. *Environ. Sci. Technol.* 2021, *55* (2), 1242-1250.
21. Qi, Y.; Li, J.; Zhang, Y.; Cao, Q.; Si, Y.; Wu, Z.; Akram, M.; Xu, X., Novel lignin-based single atom catalysts as peroxymonosulfate activator for pollutants degradation: Role of single cobalt and electron transfer pathway. *Appl. Catal. B* 2021, *286*, 119910.

22. Liu, N.; Lu, N.; Yu, H.; Chen, S.; Quan, X., Degradation of aqueous bisphenol A in the CoCN/Vis/PMS system: Catalyst design, reaction kinetic and mechanism analysis. *Chem. Eng. J.* 2021, *407*, 127228.
23. Wang, G.; Nie, X.; Ji, X.; Quan, X.; Chen, S.; Wang, H.; Yu, H.; Guo, X., Enhanced heterogeneous activation of peroxymonosulfate by Co and N codoped porous carbon for degradation of organic pollutants: the synergism between Co and N. *Environ. Sci.: Nano* 2019, *6* (2), 399-410.
24. Pan, J.; Gao, B.; Duan, P.; Guo, K.; Akram, M.; Xu, X.; Yue, Q.; Gao, Y., Improving peroxymonosulfate activation by copper ion-saturated adsorbent-based single atom catalysts for the degradation of organic contaminants: electron-transfer mechanism and the key role of Cu single atoms. *J. Mater. Chem. A* 2021, *9* (19), 11604-11613.
25. Chen, M.; Wang, N.; Zhu, L., Single-atom dispersed Co-N-C: A novel adsorption-catalysis bifunctional material for rapid removing bisphenol A. *Catal. Today* 2020, *348*, 187-193.
26. Qian, K.; Chen, H.; Li, W.; Ao, Z.; Wu, Y.-n.; Guan, X., Single-atom Fe catalyst outperforms its homogeneous counterpart for activating peroxymonosulfate to achieve effective degradation of organic contaminants. *Environ. Sci. Technol.* 2021, *55* (10), 7034-7043.
27. Gao, Y.; Zhu, Y.; Li, T.; Chen, Z.; Jiang, Q.; Zhao, Z.; Liang, X.; Hu, C., Unraveling the high-activity origin of single-atom iron catalysts for organic pollutant oxidation via peroxymonosulfate activation. *Environ. Sci. Technol.* 2021, *55* (12), 8318-8328.
28. Chen, T.; Zhu, Z.; Shen, X.; Zhang, H.; Qiu, Y.; Yin, D., Boosting peroxymonosulfate activation by porous single-atom catalysts with FeN4O1 configuration for efficient organic pollutants degradation. *Chem. Eng. J.* 2022, *450*, 138469.
29. Dong, X.; Qian, Y.; Chen, Z.; Jiang, Z.; Tang, A.; Yang, H., A nanoclay-confined single atom catalyst: tuning uncoordinated N species for efficient water treatment. *Journal of Materials Chemistry C* 2022, *10* (27), 9980-9988.
30. Liang, X.; Wang, D.; Zhao, Z.; Li, T.; Gao, Y.; Hu, C., Coordination number dependent catalytic activity of single-atom cobalt catalysts for Fenton-like reaction. *Adv. Funct. Mater.* 2022, *32* (38), 2203001.
31. Xiong, Y.; Li, H.; Liu, C.; Zheng, L.; Liu, C.; Wang, J.-O.; Liu, S.; Han, Y.; Gu, L.; Qian, J.; Wang, D., Single-atom fe catalysts for fenton-like reactions: Roles of different N species. *Adv. Mater.* 2022, *34* (17), 2110653.
32. Lu, Z.; Zhang, P.; Hu, C.; Li, F., Insights into singlet oxygen generation and electron-transfer process induced by a single-atom Cu catalyst with saturated Cu-N4 sites. *iScience* 2022, *25* (9), 104930.
33. Zuo, S.; Guan, Z.; Yang, F.; Xia, D.; Li, D., Reactive oxygen species regulation and synergistic effect for effective water purification through Fenton-like catalysis on single-atom Cu–N sites. *J. Mater. Chem. A* 2022, *10* (19), 10503-10513.